Measurement of time dependent *CP* asymmetry parameters in B^0 meson decays to ωK_S^0, $\eta' K^0$, and $\pi^0 K_S^0$

B. Aubert,[1] M. Bona,[1] Y. Karyotakis,[1] J. P. Lees,[1] V. Poireau,[1] E. Prencipe,[1] X. Prudent,[1] V. Tisserand,[1] J. Garra Tico,[2]
E. Grauges,[2] L. Lopez,[3a,3b] A. Palano,[3a,3b] M. Pappagallo,[3a,3b] G. Eigen,[4] B. Stugu,[4] L. Sun,[4] G. S. Abrams,[5] M. Battaglia,[5]
D. N. Brown,[5] R. N. Cahn,[5] R. G. Jacobsen,[5] L. T. Kerth,[5] Yu. G. Kolomensky,[5] G. Lynch,[5] I. L. Osipenkov,[5]
M. T. Ronan,[5,*] K. Tackmann,[5] T. Tanabe,[5] C. M. Hawkes,[6] N. Soni,[6] A. T. Watson,[6] H. Koch,[7] T. Schroeder,[7] D. Walker,[8]
D. J. Asgeirsson,[9] B. G. Fulsom,[9] C. Hearty,[9] T. S. Mattison,[9] J. A. McKenna,[9] M. Barrett,[10] A. Khan,[10] V. E. Blinov,[11]
A. D. Bukin,[11] A. R. Buzykaev,[11] V. P. Druzhinin,[11] V. B. Golubev,[11] A. P. Onuchin,[11] S. I. Serednyakov,[11]
Yu. I. Skovpen,[11] E. P. Solodov,[11] K. Yu. Todyshev,[11] M. Bondioli,[12] S. Curry,[12] I. Eschrich,[12] D. Kirkby,[12]
A. J. Lankford,[12] P. Lund,[12] M. Mandelkern,[12] E. C. Martin,[12] D. P. Stoker,[12] S. Abachi,[13] C. Buchanan,[13] J. W. Gary,[14]
F. Liu,[14] O. Long,[14] B. C. Shen,[14,*] G. M. Vitug,[14] Z. Yasin,[14] L. Zhang,[14] V. Sharma,[15] C. Campagnari,[16] T. M. Hong,[16]
D. Kovalskyi,[16] M. A. Mazur,[16] J. D. Richman,[16] T. W. Beck,[17] A. M. Eisner,[17] C. J. Flacco,[17] C. A. Heusch,[17]
J. Kroseberg,[17] W. S. Lockman,[17] A. J. Martinez,[17] T. Schalk,[17] B. A. Schumm,[17] A. Seiden,[17] M. G. Wilson,[17]
L. O. Winstrom,[17] C. H. Cheng,[18] D. A. Doll,[18] B. Echenard,[18] F. Fang,[18] D. G. Hitlin,[18] I. Narsky,[18] T. Piatenko,[18]
F. C. Porter,[18] R. Andreassen,[19] G. Mancinelli,[19] B. T. Meadows,[19] K. Mishra,[19] M. D. Sokoloff,[19] P. C. Bloom,[20]
W. T. Ford,[20] A. Gaz,[20] J. F. Hirschauer,[20] M. Nagel,[20] U. Nauenberg,[20] J. G. Smith,[20] K. A. Ulmer,[20] S. R. Wagner,[20]
R. Ayad,[21,†] A. Soffer,[21,‡] W. H. Toki,[21] R. J. Wilson,[21] D. D. Altenburg,[22] E. Feltresi,[22] A. Hauke,[22] H. Jasper,[22]
M. Karbach,[22] J. Merkel,[22] A. Petzold,[22] B. Spaan,[22] K. Wacker,[22] M. J. Kobel,[23] W. F. Mader,[23] R. Nogowski,[23]
K. R. Schubert,[23] R. Schwierz,[23] A. Volk,[23] D. Bernard,[24] G. R. Bonneaud,[24] E. Latour,[24] M. Verderi,[24] P. J. Clark,[25]
S. Playfer,[25] J. E. Watson,[25] M. Andreotti,[26a,26b] D. Bettoni,[26a] C. Bozzi,[26a] R. Calabrese,[26a,26b] A. Cecchi,[26a,26b]
G. Cibinetto,[26a,26b] P. Franchini,[26a,26b] E. Luppi,[26a,26b] M. Negrini,[26a,26b] A. Petrella,[26a,26b] L. Piemontese,[26a]
V. Santoro,[26a,26b] R. Baldini-Ferroli,[27] A. Calcaterra,[27] R. de Sangro,[27] G. Finocchiaro,[27] S. Pacetti,[27] P. Patteri,[27]
I. M. Peruzzi,[27,§] M. Piccolo,[27] M. Rama,[27] A. Zallo,[27] A. Buzzo,[28a] R. Contri,[28a,28b] M. Lo Vetere,[28a,28b] M. M. Macri,[28a]
M. R. Monge,[28a,28b] S. Passaggio,[28a] C. Patrignani,[28a,28b] E. Robutti,[28a] A. Santroni,[28a,28b] S. Tosi,[28a,28b]
K. S. Chaisanguanthum,[29] M. Morii,[29] A. Adametz,[30] J. Marks,[30] S. Schenk,[30] U. Uwer,[30] V. Klose,[31] H. M. Lacker,[31]
D. J. Bard,[32] P. D. Dauncey,[32] J. A. Nash,[32] M. Tibbetts,[32] P. K. Behera,[33] X. Chai,[33] M. J. Charles,[33] U. Mallik,[33]
J. Cochran,[34] H. B. Crawley,[34] L. Dong,[34] W. T. Meyer,[34] S. Prell,[34] E. I. Rosenberg,[34] A. E. Rubin,[34] Y. Y. Gao,[35]
A. V. Gritsan,[35] Z. J. Guo,[35] C. K. Lae,[35] N. Arnaud,[36] J. Béquilleux,[36] A. D'Orazio,[36] M. Davier,[36] J. Firmino da Costa,[36]
G. Grosdidier,[36] A. Höcker,[36] V. Lepeltier,[36] F. Le Diberder,[36] A. M. Lutz,[36] S. Pruvot,[36] P. Roudeau,[36] M. H. Schune,[36]
J. Serrano,[36] V. Sordini,[36,‖] A. Stocchi,[36] G. Wormser,[36] D. J. Lange,[37] D. M. Wright,[37] I. Bingham,[38] J. P. Burke,[38]
C. A. Chavez,[38] J. R. Fry,[38] E. Gabathuler,[38] R. Gamet,[38] D. E. Hutchcroft,[38] D. J. Payne,[38] C. Touramanis,[38] A. J. Bevan,[39]
C. K. Clarke,[39] K. A. George,[39] F. Di Lodovico,[39] R. Sacco,[39] M. Sigamani,[39] G. Cowan,[40] H. U. Flaecher,[40]
D. A. Hopkins,[40] S. Paramesvaran,[40] F. Salvatore,[40] A. C. Wren,[40] D. N. Brown,[41] C. L. Davis,[41] A. G. Denig,[42]
M. Fritsch,[42] W. Gradl,[42] G. Schott,[42] K. E. Alwyn,[43] D. Bailey,[43] R. J. Barlow,[43] Y. M. Chia,[43] C. L. Edgar,[43] G. Jackson,[43]
G. D. Lafferty,[43] T. J. West,[43] J. I. Yi,[43] J. Anderson,[44] C. Chen,[44] A. Jawahery,[44] D. A. Roberts,[44] G. Simi,[44] J. M. Tuggle,[44]
C. Dallapiccola,[45] X. Li,[45] E. Salvati,[45] S. Saremi,[45] R. Cowan,[46] D. Dujmic,[46] P. H. Fisher,[46] G. Sciolla,[46] M. Spitznagel,[46]
F. Taylor,[46] R. K. Yamamoto,[46] M. Zhao,[46] P. M. Patel,[47] S. H. Robertson,[47] P. Biassoni,[48a,48b] A. Lazzaro,[48a,48b]
V. Lombardo,[48a] F. Palombo,[48a,48b] J. M. Bauer,[49] L. Cremaldi,[49] R. Godang,[49,¶] R. Kroeger,[49] D. A. Sanders,[49]
D. J. Summers,[49] H. W. Zhao,[49] M. Simard,[50] P. Taras,[50] F. B. Viaud,[50] H. Nicholson,[51] G. De Nardo,[52a,52b] L. Lista,[52a]
D. Monorchio,[52a,52b] G. Onorato,[52a,52b] C. Sciacca,[52a,52b] G. Raven,[53] H. L. Snoek,[53] C. P. Jessop,[54] K. J. Knoepfel,[54]
J. M. LoSecco,[54] W. F. Wang,[54] G. Benelli,[55] L. A. Corwin,[55] K. Honscheid,[55] H. Kagan,[55] R. Kass,[55] J. P. Morris,[55]
A. M. Rahimi,[55] J. J. Regensburger,[55] S. J. Sekula,[55] Q. K. Wong,[55] N. L. Blount,[56] J. Brau,[56] R. Frey,[56] O. Igonkina,[56]
J. A. Kolb,[56] M. Lu,[56] R. Rahmat,[56] N. B. Sinev,[56] D. Strom,[56] J. Strube,[56] E. Torrence,[56] G. Castelli,[57a,57b]
N. Gagliardi,[57a,57b] M. Margoni,[57a,57b] M. Morandin,[57a] M. Posocco,[57a] M. Rotondo,[57a] F. Simonetto,[57a,57b]
R. Stroili,[57a,57b] C. Voci,[57a,57b] P. del Amo Sanchez,[58] E. Ben-Haim,[58] H. Briand,[58] G. Calderini,[58] J. Chauveau,[58]
P. David,[58] L. Del Buono,[58] O. Hamon,[58] Ph. Leruste,[58] J. Ocariz,[58] A. Perez,[58] J. Prendki,[58] S. Sitt,[58] L. Gladney,[59]
M. Biasini,[60a,60b] R. Covarelli,[60a,60b] E. Manoni,[60a,60b] C. Angelini,[61a,61b] G. Batignani,[61a,61b] S. Bettarini,[61a,61b]
M. Carpinelli,[61a,61b,**] A. Cervelli,[61a,61b] F. Forti,[61a,61b] M. A. Giorgi,[61a,61b] A. Lusiani,[61a,61c] G. Marchiori,[61a,61b]
M. Morganti,[61a,61b] N. Neri,[61a,61b] E. Paoloni,[61a,61b] G. Rizzo,[61a,61b] J. J. Walsh,[61a] D. Lopes Pegna,[62] C. Lu,[62] J. Olsen,[62]
A. J. S. Smith,[62] A. V. Telnov,[62] F. Anulli,[63a] E. Baracchini,[63a,63b] G. Cavoto,[63a] D. del Re,[63a,63b] E. Di Marco,[63a,63b]

R. Faccini,[63a,63b] F. Ferrarotto,[63a] F. Ferroni,[63a,63b] M. Gaspero,[63a,63b] P. D. Jackson,[63a] L. Li Gioi,[63a] M. A. Mazzoni,[63a] S. Morganti,[63a] G. Piredda,[63a] F. Polci,[63a,63b] F. Renga,[63a,63b] C. Voena,[63a] M. Ebert,[64] T. Hartmann,[64] H. Schröder,[64] R. Waldi,[64] T. Adye,[65] B. Franek,[65] E. O. Olaiya,[65] F. F. Wilson,[65] S. Emery,[66] M. Escalier,[66] L. Esteve,[66] S. F. Ganzhur,[66] G. Hamel de Monchenault,[66] W. Kozanecki,[66] G. Vasseur,[66] Ch. Yèche,[66] M. Zito,[66] X. R. Chen,[67] H. Liu,[67] W. Park,[67] M. V. Purohit,[67] R. M. White,[67] J. R. Wilson,[67] M. T. Allen,[68] D. Aston,[68] R. Bartoldus,[68] P. Bechtle,[68] J. F. Benitez,[68] R. Cenci,[68] J. P. Coleman,[68] M. R. Convery,[68] J. C. Dingfelder,[68] J. Dorfan,[68] G. P. Dubois-Felsmann,[68] W. Dunwoodie,[68] R. C. Field,[68] A. M. Gabareen,[68] S. J. Gowdy,[68] M. T. Graham,[68] P. Grenier,[68] C. Hast,[68] W. R. Innes,[68] J. Kaminski,[68] M. H. Kelsey,[68] H. Kim,[68] P. Kim,[68] M. L. Kocian,[68] D. W. G. S. Leith,[68] S. Li,[68] B. Lindquist,[68] S. Luitz,[68] V. Luth,[68] H. L. Lynch,[68] D. B. MacFarlane,[68] H. Marsiske,[68] R. Messner,[68] D. R. Muller,[68] H. Neal,[68] S. Nelson,[68] C. P. O'Grady,[68] I. Ofte,[68] A. Perazzo,[68] M. Perl,[68] B. N. Ratcliff,[68] A. Roodman,[68] A. A. Salnikov,[68] R. H. Schindler,[68] J. Schwiening,[68] A. Snyder,[68] D. Su,[68] M. K. Sullivan,[68] K. Suzuki,[68] S. K. Swain,[68] J. M. Thompson,[68] J. Va'vra,[68] A. P. Wagner,[68] M. Weaver,[68] C. A. West,[68] W. J. Wisniewski,[68] M. Wittgen,[68] D. H. Wright,[68] H. W. Wulsin,[68] A. K. Yarritu,[68] K. Yi,[68] C. C. Young,[68] V. Ziegler,[68] P. R. Burchat,[69] A. J. Edwards,[69] S. A. Majewski,[69] T. S. Miyashita,[69] B. A. Petersen,[69] L. Wilden,[69] S. Ahmed,[70] M. S. Alam,[70] J. A. Ernst,[70] B. Pan,[70] M. A. Saeed,[70] S. B. Zain,[70] S. M. Spanier,[71] B. J. Wogsland,[71] R. Eckmann,[72] J. L. Ritchie,[72] A. M. Ruland,[72] C. J. Schilling,[72] R. F. Schwitters,[72] B. W. Drummond,[73] J. M. Izen,[73] X. C. Lou,[73] F. Bianchi,[74a,74b] D. Gamba,[74a,74b] M. Pelliccioni,[74a,74b] M. Bomben,[75a,75b] L. Bosisio,[75a,75b] C. Cartaro,[75a,75b] G. Della Ricca,[75a,75b] L. Lanceri,[75a,75b] L. Vitale,[75a,75b] V. Azzolini,[76] N. Lopez-March,[76] F. Martinez-Vidal,[76] D. A. Milanes,[76] A. Oyanguren,[76] J. Albert,[77] Sw. Banerjee,[77] B. Bhuyan,[77] H. H. F. Choi,[77] K. Hamano,[77] R. Kowalewski,[77] M. J. Lewczuk,[77] I. M. Nugent,[77] J. M. Roney,[77] R. J. Sobie,[77] T. J. Gershon,[78] P. F. Harrison,[78] J. Ilic,[78] T. E. Latham,[78] G. B. Mohanty,[78] H. R. Band,[79] X. Chen,[79] S. Dasu,[79] K. T. Flood,[79] Y. Pan,[79] M. Pierini,[79] R. Prepost,[79] C. O. Vuosalo,[79] and S. L. Wu[79]

(*BABAR* Collaboration)

[1]*Laboratoire de Physique des Particules, IN2P3/CNRS et Université de Savoie, F-74941 Annecy-Le-Vieux, France*
[2]*Universitat de Barcelona, Facultat de Fisica, Departament ECM, E-08028 Barcelona, Spain*
[3a]*INFN Sezione di Bari, I-70126 Bari, Italy*
[3b]*Dipartimento di Fisica, Università di Bari, I-70126 Bari, Italy*
[4]*University of Bergen, Institute of Physics, N-5007 Bergen, Norway*
[5]*Lawrence Berkeley National Laboratory and University of California, Berkeley, California 94720, USA*
[6]*University of Birmingham, Birmingham, B15 2TT, United Kingdom*
[7]*Ruhr Universität Bochum, Institut für Experimentalphysik 1, D-44780 Bochum, Germany*
[8]*University of Bristol, Bristol BS8 1TL, United Kingdom*
[9]*University of British Columbia, Vancouver, British Columbia, Canada V6T 1Z1*
[10]*Brunel University, Uxbridge, Middlesex UB8 3PH, United Kingdom*
[11]*Budker Institute of Nuclear Physics, Novosibirsk 630090, Russia*
[12]*University of California at Irvine, Irvine, California 92697, USA*
[13]*University of California at Los Angeles, Los Angeles, California 90024, USA*
[14]*University of California at Riverside, Riverside, California 92521, USA*
[15]*University of California at San Diego, La Jolla, California 92093, USA*
[16]*University of California at Santa Barbara, Santa Barbara, California 93106, USA*
[17]*University of California at Santa Cruz, Institute for Particle Physics, Santa Cruz, California 95064, USA*
[18]*California Institute of Technology, Pasadena, California 91125, USA*
[19]*University of Cincinnati, Cincinnati, Ohio 45221, USA*
[20]*University of Colorado, Boulder, Colorado 80309, USA*
[21]*Colorado State University, Fort Collins, Colorado 80523, USA*
[22]*Technische Universität Dortmund, Fakultät Physik, D-44221 Dortmund, Germany*
[23]*Technische Universität Dresden, Institut für Kernund Teilchenphysik, D-01062 Dresden, Germany*
[24]*Laboratoire Leprince-Ringuet, CNRS/IN2P3, Ecole Polytechnique, F-91128 Palaiseau, France*
[25]*University of Edinburgh, Edinburgh EH9 3JZ, United Kingdom*
[26a]*INFN Sezione di Ferrara, I-44100 Ferrara, Italy*
[26b]*Dipartimento di Fisica, Università di Ferrara, I-44100 Ferrara, Italy*
[27]*INFN Laboratori Nazionali di Frascati, I-00044 Frascati, Italy*
[28a]*INFN Sezione di Genova, I-16146 Genova, Italy*
[28b]*Dipartimento di Fisica, Università di Genova, I-16146 Genova, Italy*
[29]*Harvard University, Cambridge, Massachusetts 02138, USA*

[30]*Universität Heidelberg, Physikalisches Institut, Philosophenweg 12, D-69120 Heidelberg, Germany*

[31]*Humboldt-Universität zu Berlin, Institut für Physik, Newtonstr. 15, D-12489 Berlin, Germany*

[32]*Imperial College London, London, SW7 2AZ, United Kingdom*

[33]*University of Iowa, Iowa City, Iowa 52242, USA*

[34]*Iowa State University, Ames, Iowa 50011-3160, USA*

[35]*Johns Hopkins University, Baltimore, Maryland 21218, USA*

[36]*Laboratoire de l'Accélérateur Linéaire, IN2P3/CNRS et Université Paris-Sud 11,*
Centre Scientifique d'Orsay, B. P. 34, F-91898 Orsay Cedex, France

[37]*Lawrence Livermore National Laboratory, Livermore, California 94550, USA*

[38]*University of Liverpool, Liverpool L69 7ZE, United Kingdom*

[39]*Queen Mary, University of London, London, E1 4NS, United Kingdom*

[40]*University of London, Royal Holloway and Bedford New College, Egham, Surrey TW20 0EX, United Kingdom*

[41]*University of Louisville, Louisville, Kentucky 40292, USA*

[42]*Johannes Gutenberg-Universität Mainz, Institut für Kernphysik, D-55099 Mainz, Germany*

[43]*University of Manchester, Manchester M13 9PL, United Kingdom*

[44]*University of Maryland, College Park, Maryland 20742, USA*

[45]*University of Massachusetts, Amherst, Massachusetts 01003, USA*

[46]*Massachusetts Institute of Technology, Laboratory for Nuclear Science, Cambridge, Massachusetts 02139, USA*

[47]*McGill University, Montréal, Québec, Canada H3A 2T8*

[48a]*INFN Sezione di Milano, I-20133 Milano, Italy;*

[48b]*Dipartimento di Fisica, Università di Milano, I-20133 Milano, Italy*

[49]*University of Mississippi, University, Mississippi 38677, USA*

[50]*Université de Montréal, Physique des Particules, Montréal, Québec, Canada H3C 3J7*

[51]*Mount Holyoke College, South Hadley, Massachusetts 01075, USA*

[52a]*INFN Sezione di Napoli, I-80126 Napoli, Italy;*

[52b]*Dipartimento di Scienze Fisiche, Università di Napoli Federico II, I-80126 Napoli, Italy*

[53]*NIKHEF, National Institute for Nuclear Physics and High Energy Physics, NL-1009 DB Amsterdam, The Netherlands*

[54]*University of Notre Dame, Notre Dame, Indiana 46556, USA*

[55]*Ohio State University, Columbus, Ohio 43210, USA*

[56]*University of Oregon, Eugene, Oregon 97403, USA*

[57a]*INFN Sezione di Padova, I-35131 Padova, Italy;*

[57b]*Dipartimento di Fisica, Università di Padova, I-35131 Padova, Italy*

[58]*Laboratoire de Physique Nucléaire et de Hautes Energies, IN2P3/CNRS, Université Pierre, et*
Marie Curie-Paris6, Université Denis Diderot-Paris7, F-75252 Paris, France

[59]*University of Pennsylvania, Philadelphia, Pennsylvania 19104, USA*

[60a]*INFN Sezione di Perugia, I-06100 Perugia, Italy;*

[60b]*Dipartimento di Fisica, Università di Perugia, I-06100 Perugia, Italy*

[61a]*INFN Sezione di Pisa, I-56127 Pisa, Italy;*

[61b]*Dipartimento di Fisica, Università di Pisa, I-56127 Pisa, Italy;*

[61c]*Scuola Normale Superiore di Pisa, I-56127 Pisa, Italy*

[62]*Princeton University, Princeton, New Jersey 08544, USA*

[63a]*INFN Sezione di Roma, I-00185 Roma, Italy;*

[63b]*Dipartimento di Fisica, Università di Roma La Sapienza, I-00185 Roma, Italy*

[64]*Universität Rostock, D-18051 Rostock, Germany*

[65]*Rutherford Appleton Laboratory, Chilton, Didcot, Oxon, OX11 0QX, United Kingdom*

[66]*CEA, Irfu, SPP, Centre de Saclay, F-91191 Gif-sur-Yvette, France*

[67]*University of South Carolina, Columbia, South Carolina 29208, USA*

[68]*Stanford Linear Accelerator Center, Stanford, California 94309, USA*

[69]*Stanford University, Stanford, California 94305-4060, USA*

[70]*State University of New York, Albany, New York 12222, USA*

[71]*University of Tennessee, Knoxville, Tennessee 37996, USA*

[72]*University of Texas at Austin, Austin, Texas 78712, USA*

[*]Deceased.

[†]Now at Temple University, Philadelphia, PA 19122, USA.

[‡]Now at Tel Aviv University, Tel Aviv, 69978, Israel.

[§]Also with Università di Perugia, Dipartimento di Fisica, Perugia, Italy.

[‖]Also with Università di Roma La Sapienza, I-00185 Roma, Italy.

[¶]Now at University of South Alabama, Mobile, AL 36688, USA.

[**]Also with Università di Sassari, Sassari, Italy.

[73]*University of Texas at Dallas, Richardson, Texas 75083, USA*
[74a]*INFN Sezione di Torino, I-10125 Torino, Italy;*
[74b]*Dipartimento di Fisica Sperimentale, Università di Torino, I-10125 Torino, Italy*
[75a]*INFN Sezione di Trieste, I-34127 Trieste, Italy;*
[75b]*Dipartimento di Fisica, Università di Trieste, I-34127 Trieste, Italy*
[76]*IFIC, Universitat de Valencia-CSIC, E-46071 Valencia, Spain*
[77]*University of Victoria, Victoria, British Columbia, Canada V8W 3P6*
[78]*Department of Physics, University of Warwick, Coventry CV4 7AL, United Kingdom*
[79]*University of Wisconsin, Madison, Wisconsin 53706, USA*

We present measurements of the time-dependent CP-violation parameters S and C in the decays $B^0 \rightarrow \omega K_S^0$, $B^0 \rightarrow \eta' K^0$, reconstructed as $\eta' K_S^0$ and $\eta' K_L^0$, and $B^0 \rightarrow \pi^0 K_S^0$. The data sample corresponds to the full *BABAR* dataset of 467×10^6 $B\bar{B}$ pairs produced at the PEP-II asymmetric-energy $e^+ e^-$ collider at the Stanford Linear Accelerator Center. The results are $S_{\omega K_S^0} = 0.55^{+0.26}_{-0.29} \pm 0.02$, $C_{\omega K_S^0} = -0.52^{+0.22}_{-0.20} \pm 0.03$, $S_{\eta' K^0} = 0.57 \pm 0.08 \pm 0.02$, $C_{\eta' K^0} = -0.08 \pm 0.06 \pm 0.02$, $S_{\pi^0 K_S^0} = 0.55 \pm 0.20 \pm 0.03$, and $C_{\pi^0 K_S^0} = 0.13 \pm 0.13 \pm 0.03$, where the first errors are statistical and the second systematic. These results are consistent with our previous measurements and the world average of $\sin 2\beta$ measured in $B^0 \rightarrow J/\psi K_S^0$.

I. INTRODUCTION

Measurements of time-dependent CP asymmetries in B^0 meson decays through $b \rightarrow c\bar{c}s$ amplitudes have provided crucial tests of the mechanism of CP violation in the standard model (SM) [1]. These amplitudes contain the leading b-quark couplings, given by the Cabibbo-Kobayashi-Maskawa [2] (CKM) flavor mixing matrix, for kinematically allowed transitions. Decays to charmless final states such as ϕK^0, $\pi^0 K^0$, $\eta' K^0$, ωK^0, $K^+ K^- K^0$, $f_0(980)K^0$ are CKM-suppressed $b \rightarrow q\bar{q}s$ ($q = u$, d, s) processes dominated by a single loop (penguin) amplitude. This amplitude has the same weak phase $\beta = \arg(-V_{cd}V_{cb}^*/V_{td}V_{tb}^*)$ of the CKM-mixing matrix as that measured in the $b \rightarrow c\bar{c}s$ transition, but is sensitive to the possible presence of new heavy particles in the loop [3]. Because of the different nonperturbative strong-interaction properties of the various penguin decays, the effect of new physics is expected to be channel dependent.

The CKM phase β is accessible experimentally through interference between the direct decay of the B meson to a CP eigenstate and $B^0\bar{B}^0$ mixing followed by decay to the same final state. This interference is observable through the time evolution of the decay. In the present study, we reconstruct one B^0 from $\Upsilon(4S) \rightarrow B^0\bar{B}^0$, which decays to the CP eigenstate ωK_S^0, $\eta' K_S^0$, $\eta' K_L^0$, or $\pi^0 K_S^0$ (B_{CP}). From the remaining particles in the event we also reconstruct the decay vertex of the other B meson (B_{tag}) and identify its flavor. The distribution of the difference $\Delta t \equiv t_{CP} - t_{tag}$ of the proper decay times t_{CP} and t_{tag} of these mesons is given by

$$f(\Delta t) = \frac{e^{-|\Delta t|/\tau}}{4\tau}\{1 \pm [-\eta_f S_f \sin(\Delta m_d \Delta t) \\ - C_f \cos(\Delta m_d \Delta t)]\}, \quad (1)$$

where η_f is the CP eigenvalue of final state f (-1 for ωK_S^0, $\eta' K_S^0$, and $\pi^0 K_S^0$; $+1$ for $\eta' K_L^0$). The upper (lower) sign denotes a decay accompanied by a $B^0(\bar{B}^0)$ tag, τ is the mean B^0 lifetime, and Δm_d is the mixing frequency.

A nonzero value of the parameter C_f would indicate direct CP violation. In these modes we expect $C_f = 0$ and $-\eta_f S_f = \sin 2\beta$, assuming penguin dominance of the $b \rightarrow s$ transition and neglecting other CKM-suppressed amplitudes with a different weak phase. However, these CKM-suppressed amplitudes and the color-suppressed tree diagram introduce additional weak phases whose contributions may not be negligible [4–7]. As a consequence, the measured S_f may differ from $\sin 2\beta$ even within the SM. This deviation $\Delta S_f = S_f - \sin 2\beta$ is estimated in several theoretical approaches: QCD factorization (QCDF) [4,8], QCDF with modeled rescattering [9], soft collinear effective theory [10], and SU(3) symmetry [5,7,11]. The estimates are channel dependent. Estimates of ΔS from QCDF are in the ranges (0.0, 0.2), (−0.03, 0.03), and (0.01, 0.12) for ωK_S^0, $\eta' K^0$, and $\pi^0 K_S^0$, respectively [8,10,12]; SU(3) symmetry provides bounds of (−0.05, 0.09) for $\eta' K^0$ and (−0.06, 0.12) for $\pi^0 K_S^0$ [11]. Predictions that use isospin symmetry to relate several amplitudes, including the $I = \frac{3}{2} B \rightarrow K\pi$ amplitude, give an expected value for $S_{\pi^0 K_S^0}$ near 1.0 instead of $\sin 2\beta$ [13].

We present updated measurements of mixing-induced CP violation in the B^0 decay modes ωK_S^0, $\eta' K^0$, and $\pi^0 K_S^0$, which supersede our previous measurements [14–16]. Significant changes to previous analyses include twice as much data for ωK_S^0, 20% more data for $\eta' K^0$ and $\pi^0 K_S^0$, improved track reconstruction, and an additional decay channel in $\eta' K_L^0$. Despite the modest increase in data, the uncertainties on $S_{\eta' K^0}$ and $C_{\eta' K^0}$ decrease by 20% and 25%, respectively. Measurements in these modes have also been made by the Belle Collaboration [17,18].

II. THE *BABAR* DETECTOR AND DATASET

The results presented in this paper are based on data collected with the *BABAR* detector at the PEP-II asymmetric-energy e^+e^- storage ring, operating at the Stanford Linear Accelerator Center. At PEP-II, 9.0 GeV electrons collide with 3.1 GeV positrons to yield a center-of-mass energy of $\sqrt{s} = 10.58$ GeV, which corresponds to the mass of the $Y(4S)$ resonance. The asymmetric energies result in a boost from the laboratory to the e^+e^- center-of-mass frame of $\beta\gamma \approx 0.56$. We analyze the entire *BABAR* dataset collected at the $Y(4S)$ resonance, corresponding to an integrated luminosity of 426 fb^{-1} and $(467 \pm 5) \times 10^6$ $B\bar{B}$ pairs. We use an additional 44 fb^{-1} of data recorded about 40 MeV below this energy (off-peak) for the study of the non-$B^0\bar{B}^0$ background.

A detailed description of the *BABAR* detector can be found elsewhere [19]. Surrounding the interaction point is a five-layer double-sided silicon vertex tracker (SVT) that provides precision measurements near the collision point of charged particle tracks in the planes transverse to and along the beam direction. A 40-layer drift chamber surrounds the SVT. Both of these tracking devices operate in the 1.5 T magnetic field of a superconducting solenoid to provide measurements of the momenta of charged particles. Charged hadron identification is achieved through measurements of particle energy loss in the tracking system and the Cherenkov angle obtained from a detector of internally reflected Cherenkov light. A CsI(Tl) electromagnetic calorimeter (EMC) provides photon detection, electron identification, and π^0, η, and K_L^0 reconstruction. Finally, the instrumented flux return (IFR) of the magnet allows discrimination of muons from pions and detection of K_L^0 mesons. For the first 214 fb^{-1} of data, the IFR was composed of a resistive plate chamber system. For the most recent 212 fb^{-1} of data, a portion of the resistive plate chamber system has been replaced by limited streamer tubes [20].

III. VERTEX RECONSTRUCTION

In the reconstruction of the B_{CP} vertex, we use all charged daughter tracks. Daughter tracks that form a K_S^0 are fit to a separate vertex, with the resulting parent momentum and position used in the fit to the B_{CP} vertex. The vertex for the B_{tag} decay is constructed from all tracks in the event except the daughters of B_{CP}. An additional constraint is provided by the calculated B_{tag} production point and three-momentum, with its associated error matrix. This is determined from the knowledge of the three-momentum of the fully reconstructed B_{CP} candidate, its decay vertex and error matrix, and from the knowledge of the average position of the e^+e^- interaction point and $Y(4S)$ average boost. In order to reduce bias and tails due to long-lived particles, K_S^0 and Λ^0 candidates are used as input to the fit in place of their daughters. In addition, tracks consistent

with photon conversions ($\gamma \rightarrow e^+e^-$) are excluded from the fit. To reduce contributions from charm decay products that bias the determination of the vertex position the tracks with a vertex χ^2 contribution greater than 6 are removed and the fit is repeated until no track fails the χ^2 requirement. We obtain Δt from the measured distance Δz between the B_{CP} and B_{tag} vertex with the relation $\Delta z \simeq \beta\gamma c\Delta t$.

Because there are no charged particles present at the $B^0 \rightarrow \pi^0 K_S^0$ decay vertex, the $\pi^0 K_S^0$ vertex reconstruction differs significantly from that of the ωK_S^0 and $\eta' K^0$ analyses. In $\pi^0 K_S^0$ we identify the vertex of the B_{CP} using the single K_S^0 trajectory from the $\pi^+\pi^-$ momenta and the knowledge of the average interaction point (IP) [21], which is determined several times per hour from the spatial distribution of vertices from two track events. The average transverse size of the IP is 180 $\mu m \times 4$ μm. We compute Δt and its uncertainty with a geometric fit to the $Y(4S) \rightarrow B^0\bar{B}^0$ system that takes this IP constraint into account. We further improve the accuracy of the Δt measurement by constraining the sum of the two B decay times ($t_{CP} + t_{tag}$) to be equal to 2τ (τ is the mean B^0 lifetime) with an uncertainty $\sqrt{2}\tau$, which effectively improves the determination of the decay position of the $Y(4S)$. We have verified in a full detector simulation that this procedure provides an unbiased estimate of Δt.

The estimate of the uncertainty on Δt for each $\pi^0 K_S^0$ event reflects the strong dependence of the Δt resolution on the K_S^0 flight direction and on the number of SVT layers traversed by the K_S^0 decay daughters. When both pion tracks are reconstructed with information from at least the first three layers of the SVT in the coordinate along the collision axis (axial) as well as on the transverse plane (azimuthal), we obtain Δt with resolution comparable to that of the ωK_S^0 and $\eta' K^0$ analyses. The average Δt resolution in these modes is about 1.0 ps. Events for which there is axial and azimuthal information from the first three layers of the SVT and for which Δt and the error on Δt satisfy $|\Delta t| < 20$ ps and $\sigma_{\Delta t} < 2.5$ ps are classified as "good" (class g), and their Δt information is used in the time-dependent part of the likelihood function Eq. (10). About 60% of the events fall in this class. Otherwise events are classified as "bad" (class b). Since C_f can also be extracted from flavor tagging information alone, events of class b contribute to the measurement of C_f Eq. (11) and to the signal yield in the $\pi^0 K_S^0$ analysis.

In ωK_S^0 and $\eta' K^0$ decays, the determination of the B decay vertex is dominated by the charged daughters of the ω and η', so we do not require information in the first three SVT layers from K_S^0 daughter pions for events in class g. Also, since about 95% of events in these modes are of class g, the precision of the measurement of C_f is not improved by including class b events. We maintain simplicity of these analyses by simply rejecting class b events.

IV. FLAVOR TAGGING AND Δt RESOLUTION

In the measurement of time-dependent *CP* asymmetries, it is important to determine whether at the time of decay of the B_{tag} the B_{CP} was a B^0 or a $\bar{B}^0$. This "flavor tagging" is achieved with the analysis of the decay products of the recoiling B_{tag} meson. Most *B* mesons decay to a final state that is flavor specific; i.e., only accessible from either a B^0 or a $\bar{B}^0$, but not from both. The purpose of the flavor tagging algorithm is to determine the flavor of B_{tag} with the highest possible efficiency ϵ and lowest possible probability w of assigning a wrong flavor to B_{tag}. The figure of merit for the performance of the tagging algorithm is the effective tagging efficiency

$$Q = \epsilon(1 - 2w)^2, \qquad (2)$$

which is approximately related to the statistical uncertainty σ in the coefficients S and C through

$$\sigma \propto \frac{1}{\sqrt{Q}}. \qquad (3)$$

It is not necessary to reconstruct B_{tag} fully to determine its flavor. We use a neural network based technique [22] to exploit signatures of *B* decays that determine the flavor at decay of the B_{tag}. Primary leptons from semileptonic *B* decays are selected from identified electrons and muons as well as isolated energetic tracks. The charges of identified kaon candidates define a kaon tag. Soft pions from D^{*+} decays are selected on the basis of their momentum and direction with respect to the thrust axis of B_{tag}. Based on the output of this algorithm, candidates are divided into seven mutually exclusive categories. These are (in order of decreasing signal purity) `Lepton`, `Kaon I`, `Kaon II`, `Kaon-Pion`, `Pion`, `Other`, and `Untagged`.

We apply this algorithm to a sample of fully reconstructed, self-tagging, neutral *B* decays (B_{flav} sample). We use *B* decays to $D^{(*)-}(\pi^+, \rho^+, a_1^+)$ to measure the tagging efficiency ϵ, mistag rate w, and the difference in mistag rates for B^0 and $\bar{B}^0$ tagside decays $\Delta w \equiv w(B^0) - w(\bar{B}^0)$. The results are shown in Table I. The `Untagged` category of events contains no flavor information and

TABLE I. Efficiencies ε, average mistag fractions w, mistag fraction differences $\Delta w \equiv w(B^0) - w(\bar{B}^0)$, and effective tagging efficiency $Q \equiv \epsilon(1 - 2w)^2$ for each tagging category from the B_{flav} data.

Category	ε (%)	w (%)	Δw (%)	Q (%)
Lepton	9.0 ± 0.1	2.8 ± 0.3	0.3 ± 0.5	8.0 ± 0.1
Kaon I	10.8 ± 0.1	5.3 ± 0.3	-0.1 ± 0.6	8.7 ± 0.1
Kaon II	17.2 ± 0.1	14.5 ± 0.3	0.4 ± 0.6	8.7 ± 0.2
Kaon-Pion	13.7 ± 0.1	23.3 ± 0.4	-0.7 ± 0.7	3.9 ± 0.1
Pion	14.2 ± 0.1	32.5 ± 0.4	5.1 ± 0.7	1.7 ± 0.1
Other	9.5 ± 0.1	41.5 ± 0.5	3.8 ± 0.8	0.3 ± 0.0
All	74.4 ± 0.1			31.2 ± 0.3

therefore carries no weight in the time-dependent analysis. The total effective tagging efficiency Q for this algorithm is measured to be $(31.2 \pm 0.3)\%$.

Including the effects of the mistag rate, Eq. (1) becomes

$$F(\Delta t) = \frac{e^{-|\Delta t|/\tau}}{4\tau}\{1 \mp \Delta w \pm (1 - 2w)$$
$$\times [-\eta_f S_f \sin(\Delta m_d \Delta t) - C_f \cos(\Delta m_d \Delta t)]\}. \qquad (4)$$

Finally, to account for experimental Δt resolution, we convolve Eq. (4) with a resolution function, the parameters of which we obtain from fits to the B_{flav} sample. The Δt resolution function is represented as a sum of three Gaussian distributions with different widths. For the core and tail Gaussians, the widths are scaled by $\sigma_{\Delta t}$. In addition we allow an offset for the core distribution in the hadronic tagging categories (Sec. IV) separate from that of the `Lepton` category, to allow for a small bias of Δt from secondary *D*-meson decays; a common offset is used for the tail component. The third Gaussian (of fixed 8 ps width) accounts for the few events with incorrectly reconstructed vertices. Identical resolution function parameters are used for all B_{CP} modes, since the B_{tag} vertex precision dominates the Δt resolution.

Events without reliable Δt information (class *b*) are sensitive to the parameter C_f and are used to constrain this parameter in the $\pi^0 K_S^0$ analysis. Integrating Eq. (4) over Δt we get

$$F^C = \frac{1}{2}\{1 \mp [\Delta w + C_f(1 - 2w)/(1 + \Delta m_d^2\tau^2)]\}. \qquad (5)$$

We also account for the asymmetry in tagging efficiency for B^0 and $\bar{B}^0$ decays, but, for simplicity, we assume the asymmetry is zero in the above equations.

V. EVENT RECONSTRUCTION AND SELECTION

We choose event selection criteria with the aid of a detailed Monte Carlo (MC) simulation of the *B* production and decay sequences, and of the detector response [23]. These criteria are designed to retain signal events with high efficiency while removing most of the background.

We reconstruct the B_{CP} candidate by combining the four-momenta of the two daughter mesons, with a vertex constraint. The *B*-daughter candidates are reconstructed with the following decays: $\pi^0 \to \gamma\gamma$; $\eta \to \gamma\gamma(\eta_{\gamma\gamma})$; $\eta \to \pi^+\pi^-\pi^0(\eta_{3\pi})$; $\eta' \to \eta_{\gamma\gamma}\pi^+\pi^-(\eta'_{\eta(\gamma\gamma)\pi\pi})$; $\eta' \to \eta_{3\pi}\pi^+\pi^-(\eta'_{\eta(3\pi)\pi\pi})$; $\eta' \to \rho^0\gamma(\eta'_{\rho\gamma})$, where $\rho^0 \to \pi^+\pi^-$; $\omega \to \pi^+\pi^-\pi^0$; and $K_S^0 \to \pi^+\pi^-(K_{\pi^+\pi^-}^0)$. In the $\eta'K_S^0$ analysis we also reconstruct K_S^0 via its decay to two neutral pions ($K_{\pi^0\pi^0}^0$). The requirements on the invariant masses of these particle combinations are given in Table II. We consider as photons energy depositions in the EMC that are isolated from any charged tracks, carry a minimum

TABLE II.   Selection requirements on the invariant masses of candidate resonant decays and the laboratory energies of photons from the decay.

State	Invariant mass (MeV)	$E(\gamma)$ (MeV)
Prompt π^0	$110 < m(\gamma\gamma) < 160$	>50
Secondary π^0	$120 < m(\gamma\gamma) < 150$	>30
$\eta_{\gamma\gamma}$	$490 < m(\gamma\gamma) < 600$	>50
$\eta_{3\pi}$	$520 < m(\pi^+\pi^-\pi^0) < 570$	-
$\eta'_{\eta\pi\pi}$	$945 < m(\pi^+\pi^-\eta) < 970$	-
$\eta'_{\rho\gamma}$	$930 < m(\pi^+\pi^-\gamma) < 980$	>100
ω	$735 < m(\pi^+\pi^-\pi^0) < 825$	-
ρ^0	$470 < m(\pi^+\pi^-) < 980$	-
$K^0_{\pi^+\pi^-}$	$486 < m(\pi^+\pi^-) < 510$	-
$K^0_{\pi^0\pi^0}$	$468 < m(\pi^0\pi^0) < 528$	-

energy of 30 MeV, and have the expected lateral shower shapes.

The five final states used for $B^0 \to \eta'K^0_S$ are $\eta'_{\eta(\gamma\gamma)\pi\pi}K^0_{\pi^+\pi^-}$, $\eta'_{\rho\gamma}K^0_{\pi^+\pi^-}$, $\eta'_{\eta(3\pi)\pi\pi}K^0_{\pi^+\pi^-}$, $\eta'_{\eta(\gamma\gamma)\pi\pi}K^0_{\pi^0\pi^0}$, and $\eta'_{\rho\gamma}K^0_{\pi^0\pi^0}$. For the $B^0 \to \eta'K^0_L$ channel we reconstruct the η' in two modes: $\eta'_{\eta(\gamma\gamma)\pi\pi}$ and $\eta'_{\eta(3\pi)\pi\pi}$. Large backgrounds to the final states $\eta'_{\rho\gamma}K^0_L$, ωK^0_L, and $\omega K^0_{\pi^0\pi^0}$ preclude these modes from improving the precision of the measurement of *CP* parameters in $\eta'K^0$ and ωK^0; $\pi^0 K^0_L$ and $\pi^0 K^0_{\pi^0\pi^0}$ events lack the minimum information for reconstruction of the decay vertex.

For decays with a $K^0_S \to \pi^+\pi^-$ candidate we perform a fit of the entire decay tree which constrains the K^0_S flight direction to the pion pair momentum direction and the K^0_S production point to the B_{CP} vertex determined as described in Sec. III. In this vertex fit we also constrain the η, η', and π^0 candidate masses to world-average values [24], since these resonances have natural widths that are negligible compared to the resolution. Given that the natural widths of the ω and ρ mesons are comparable to or greater than the detector resolution, we do not impose any constraint on the masses of these candidates; constraining the mass of the K^0_S does not improve determination of the vertex. In the ωK^0_S and $\eta'K^0_S$ analyses, we require the χ^2 probability of this fit to be greater than 0.001. We also require that the K^0_S flight length divided by its uncertainty be greater than 3.0 (5.0 for $B^0 \to \pi^0 K^0_S$).

Signal K^0_L candidates are reconstructed from clusters of energy deposited in the EMC or from hits in the IFR not associated with any charged track in the event [25]. Taking the flight direction of the K^0_L to be the direction from the B^0 decay vertex to the cluster centroid, we determine the K^0_L momentum $\mathbf{p}_{K^0_L}$ from a fit with the B^0 and K^0_L masses constrained to world-average values [24].

A. Kinematics of $Y(4S) \to B\bar{B}$

In this experiment the energy of the initial e^+e^- state is known within an uncertainty of a few MeV. For a final state with two particles we can determine four kinematic variables from conservation of energy and momentum. These may be taken as polar and azimuthal angles of the line of flight of the two particles, and two energy, momentum, or mass variables, such as the masses of the two particles. In practice, since we fully reconstruct one B meson candidate, we make the assumption that it is one of two final-state particles of equal mass. We compute two largely uncorrelated variables that test consistency with this assumption, and with the known value [24] of the B-meson mass. The choice of these variables depends on the decay process, as we discuss below.

In the reconstruction of $B^0 \to \omega K^0_S$ and $B^0 \to \eta'K^0_S$ the kinematic variables are the energy-substituted mass

$$m_{ES} \equiv \sqrt{\left(\frac{1}{2}s + \mathbf{p}_0 \cdot \mathbf{p}_B\right)^2 / E^2_0 - \mathbf{p}^2_B} \qquad (6)$$

and the energy difference

$$\Delta E \equiv E^*_B - \frac{1}{2}\sqrt{s}, \qquad (7)$$

where $(E_0, \mathbf{p}_0)$ and $(E_B, \mathbf{p}_B)$ are the laboratory four-momenta of the $Y(4S)$ and the B_{CP} candidate, respectively, and the asterisk denotes the $Y(4S)$ rest frame. The resolution is 3 MeV in m_{ES} and 20–50 MeV in ΔE, depending on the decay mode. We require $5.25 < m_{ES} < 5.29$ GeV and $|\Delta E| < 0.2$ GeV, as distributions of these quantities for signal events peak at the B-meson mass in m_{ES} and zero in ΔE.

For the $B^0 \to \eta'K^0_L$ channel only the direction of the K^0_L momentum is measured. For these candidates m_{ES} is not determined; instead we obtain ΔE from a calculation with the B^0 and K^0_L masses constrained to world-average values. Because of the mass constraint on the B^0, the ΔE distribution for K^0_L events, which peaks at zero for signal, is asymmetric and narrower than that of K^0_S events; we require $-0.01 < \Delta E < 0.08$ GeV for $\eta'K^0_L$.

For the $\pi^0 K^0_S$ analysis we use the kinematic variables m_B and m_{miss}. The variable m_B is the invariant mass of the reconstructed B_{CP}. The variable m_{miss} is the invariant mass of the B_{tag}, computed from the known beam energy and the measured B_{CP} momentum with $m(B_{CP})$ constrained to the nominal B-meson mass m^{PDG}_B [26]. For signal decays, m_B and m_{miss} peak at the B^0 mass and have resolutions of ~ 47 MeV and ~ 5.4 MeV, respectively; the distribution of m_B exhibits a lowside tail due to leakage of energy out of the EMC. To compare the m_{miss} resolution with the m_{ES} resolution a factor of 2 from the approximate relation $m_{ES} \sim (m_{miss} + m^{PDG}_B)/2$ should be taken into account. The beam-energy constraint in m_{miss} helps to eliminate the correlation with m_B. We select candidates within the window $5.11 < m_{miss} < 5.31$ GeV and $5.13 < m_B < 5.43$ GeV, which includes the signal peak and a sideband region for background characterization.

B. Background reduction

Background events arise primarily from random combinations of particles in continuum $e^+e^- \to q\bar{q}$ events ($q = u$, d, s, c). For some of the decay chains we must also consider cross feed from B-meson decays by modes other than the signal; we discuss these in Secs. VI A and VI B below. To reduce the $q\bar{q}$ backgrounds we make use of additional properties of the event that are consequences of the decay.

For the $B^0 \to \omega K_S^0$ and $B^0 \to \eta' K^0$ channels we define the angle θ_T between the thrust axis [27] of the B_{CP} candidate in the $Y(4S)$ frame and that of the charged tracks and neutral calorimeter clusters in the rest of the event. The event is required to contain at least one charged track not associated with the B_{CP} candidate. The distribution of $|\cos\theta_T|$ is sharply peaked near 1 for $q\bar{q}$ jet pairs, and nearly uniform for B-meson decays. The requirement is $|\cos\theta_T| < 0.9$ for all modes.

For the $\eta'_{\rho\gamma}$ decays we also define the angle $\theta_{\mathrm{dec}}^\rho$ between the momenta of the ρ^0 daughter π^- and of the η', measured in the ρ^0 rest frame. We require $|\cos\theta_{\mathrm{dec}}^\rho| < 0.9$ to reduce the combinatorial background of ρ^0 candidates incorporating a soft pion that are reconstructed as decays with $|\cos\theta_{\mathrm{dec}}^\rho| \simeq 1$.

For $\eta' K_L^0$ candidates we require that the cosine of the polar angle of the total missing momentum in the laboratory system be less than 0.96 to reject very forward $q\bar{q}$ jets. We construct the missing momentum $\mathbf{p}_{\mathrm{miss}}$ as the difference of $\mathbf{p}_0$ and the momenta of all charged tracks and neutral clusters not associated with the K_L^0 candidate. We project $\mathbf{p}_{\mathrm{miss}}$ onto $\mathbf{p}_{K_L^0}$, and require the component perpendicular to the beam line, $p_{\mathrm{miss}\perp}^{\mathrm{proj}}$, to satisfy $p_{\mathrm{miss}\perp}^{\mathrm{proj}} - p_{K_L^0\perp} > -0.8$ GeV. These values are chosen to minimize the uncertainty on S and C in the presence of background.

The purity of the K_L^0 candidates reconstructed in the EMC is further improved by a requirement on the output of a neural network (NN) that takes cluster-shape variables as inputs. For the NN, we use the following eight variables: the number of crystals in the EMC cluster; the total energy deposited in the EMC cluster; the second moment of the cluster energy

$$\mu_2 = \frac{\sum_i E_i \cdot r_i^2}{\sum_i E_i}, \tag{8}$$

where E_i is the energy deposited in the ith crystal and r_i its distance from the cluster centroid; the lateral moment

$$\mu_{\mathrm{LAT}} = \frac{\sum_{i=2,n} E_i \cdot r_i^2}{\left(\sum_{i=2,n} E_i \cdot r_i^2\right) + 25(E_0 + E_1)}, \tag{9}$$

where E_0 refers to the most energetic crystal and E_n to the least energetic one; the ratio $S1/S9$ of the energy of the most energetic crystal ($S1$) to the sum of energy of the 3×3 crystal block with $S1$ in its center ($S9$); the ratio $S9/S25$,

where $S25$ is the sum of energy of the 5×5 crystal block with $S1$ in its center; and the absolute value of the expansion coefficients $|Z_{20}|$ and $|Z_{42}|$ of the spatial energy distribution of the EMC cluster expressed as a series of Zernike polynomials (ζ) : $E(x, y) = \sum_{n,m} Z_{n,m} \cdot \zeta_{n,m}(r, \phi)$, where (x, y) are the Cartesian coordinates in the plane of the calorimeter, (r, ϕ) are the polar coordinates of the Zernike polynomials ($0 \le r \le 1$) and n, m are nonnegative integers. The NN is trained on MC signal events and off-peak data reconstructed for the $\eta'_{\eta_{(\gamma\gamma)}\pi\pi} K_L^0$ decay mode to return $+1$ if the event is signal-like and -1 if it is background-like. We check the performance of the NN on an independent sample of MC signal events and off-peak data reconstructed for the $\eta'_{\eta_{(\gamma\gamma)}\pi\pi} K_L^0$ decay mode. Using ensembles of simulated experiments, as discussed in Sec. VI D, we find that requiring the output of the NN to be greater than -0.2 minimizes the average statistical uncertainty on S and C.

For the $\pi^0 K_S^0$ channel we require the χ^2 probability of the kinematic fit to be greater than 0.001. We exclude events in which the absolute value of cosine of the angle between the beam axis and the B_{CP} momentum in the $Y(4S)$ frame ($\cos\theta_B$) is greater than 0.9. Finally, we apply a cut on the event shape, selecting events with $L_2/L_0 < 0.55$; L_i is the ith angular moment defined as $L_i = \sum_j p_j \times |\cos\theta_j|^i$, where θ_j is the angle with respect to the B thrust axis of track or neutral cluster j, p_j is its momentum, and the sum excludes the daughters of the B candidate.

The average number of candidates found per selected event in $\eta' K^0$ and ωK_S^0 is between 1.08 and 1.32, depending on the final state. For events with multiple candidates we choose the one with the largest decay vertex probability for the B meson. Furthermore, in the $B^0 \to \eta' K_L^0$ sample, if several B candidates have the same vertex probability, we choose the candidate with the K_L^0 information taken from, in order, EMC and IFR, EMC only, or IFR only. From the simulation we find that this algorithm selects the correct-combination candidate in about two-thirds of the events containing multiple candidates.

For the $\pi^0 K_S^0$ channel the average number of candidates found per selected event is 1.03. In events with multiple candidates we choose the one with the smallest value of χ^2 obtained from the reconstructed mass of the K_S^0 and the π^0 candidates and their respective errors.

In the $\eta' K^0$ analysis, we estimate from MC the fraction of events in which we misreconstruct charged daughters of the η' (self-crossfeed events), which dominate the determination of the B_{CP} decay vertex. We find that $(1–4)\%$ of events are self-crossfeed, depending on the η' and K^0 decay channel.

VI. MAXIMUM LIKELIHOOD FIT

The selected sample sizes are given in the table of results in Sec. VII. We perform an unbinned maximum likelihood

(ML) fit to these data to obtain the common *CP*-violation parameters and signal yields for each channel. For each signal or background component j, tagging category c, and event class $t = g$ (Sec. III), we define a total probability density function (PDF) for event i as

$$\mathcal{P}^i_{j,c,g} \equiv \mathcal{T}_{j,c}(\Delta t^i, \sigma^i_{\Delta t}, \varphi^i) \cdot \prod_k \mathcal{Q}_{k,j}(x^i_k), \qquad (10)$$

where $\mathcal{T}$ is the function $F(\Delta t)$ defined in Eq. (4) convolved with the Δt resolution function, and $\varphi = \pm 1$ is the B flavor defined by upper and lower signs in Eq. (1). For event class $t = b$ (for the $\pi^0 K^0_S$ analysis), we define a total PDF for event i as

$$\mathcal{P}^i_{j,c,b} \equiv F^C_{j,c}(\varphi^i) \cdot \prod_k \mathcal{Q}_{k,j}(x^i_k), \qquad (11)$$

where F^C is the function defined in Eq. (5). The set of variables x^i_k, which serve to discriminate signal from background, are described along with their PDFs $\mathcal{Q}_{k,j}(x_k)$ in Sec. VI B below. The factored form of the PDF is a good approximation since linear correlations are smaller than 5%, 7%, and 6% in the ωK^0_S, $\eta' K^0$, and $\pi^0 K^0_S$ analyses, respectively. The effects of these correlations are estimated as described in Sec. VI D.

We write the extended likelihood function for all candidates for decay mode d as

$$\mathcal{L}_d = \prod_{c,t} \frac{\exp(-\sum_j n_j f_{j,t} \epsilon_{j,c})}{N_{c,t}!} \prod_i^{N_{c,t}} \left[\sum_j n_j f_{j,t} \epsilon_{j,c} \mathcal{P}^i_{j,c,t} \right], \qquad (12)$$

where n_j is the yield of events of component j, $f_{j,t}$ is the fraction of events of component j for each event class t, $\epsilon_{j,c}$ is the efficiency of component j for each tagging category c, and $N_{c,t}$ is the number of events of category c with event class t in the sample. When combining decay modes we form the grand likelihood $\mathcal{L} = \prod \mathcal{L}_d$.

We fix $\epsilon_{j,c}$ for all components except the $q\bar{q}$ background to $\epsilon_{B_{\text{flav}},c}$, which are listed in Table I. For the $\pi^0 K^0_S$ channel we assume the same $\epsilon_{j,c}$ for class g and class b events. For ωK^0_S and $\eta' K^0$ we fix $f_{j,g} = 1$ because we accept only events of class g.

A. Model components

For all of the decay chains we include in the ML fit a component for $q\bar{q}$ combinatorial background ($j = q\bar{q}$), in addition to the one for the signal. The functional forms of the PDFs that describe this background are determined from fits of one observable at a time to sidebands of the data in the kinematic variables that exclude signal events. Some of the parameters of this PDF are free in the final fit. Thus, the combinatorial component receives contributions from all nonsignal events in the data.

We estimate from the simulation that charmless B decay modes contribute less than 2% of background to the input sample. These events have final states different from the signal, but similar kinematics, and exhibit broad peaks in the signal regions of some observables. We find that the charmless $B\bar{B}$ background component ($j = $ chls) is needed for the final states ωK^0_S, $\eta'_{\rho\gamma} K^0_{\pi^+\pi^-}$, and $\eta'_{\rho\gamma} K^0_{\pi^0\pi^0}$. We account for these with a separate component in the PDF. Unlike the other fit components, we fix the charmless $B\bar{B}$ yields using measured branching fractions, where available, and detection efficiencies determined from MC. For unmeasured background modes, we use theoretical estimates of branching fractions.

We also consider the presence of B decays to charmed particles in the input sample. The charmed hadrons in these final states tend to be too heavy to be misreconstructed as the two light bodies contained in our signals, and their distributions in the B kinematic variables are similar to those for $q\bar{q}$. However, in the event shape variables and Δt they are signal-like. We have found that biases in the fit results are minimized for the modes with $\eta'_{\rho\gamma}$ by including a component specifically for the B decays to charm states ($j = $ chrm). Finally, for $\eta'_{\eta(3\pi)\pi\pi} K^0_L$ we divide the signal component into two categories for correctly reconstructed and self-crossfeed events; we fix the fraction of the self-crossfeed category to the value obtained from MC.

B. Probability density functions

The set of variables x_k of Eqs. (10) and (11) is defined for each family of decays as

(i) $B^0 \rightarrow \omega K^0_S$: $\{ m_{\text{ES}}, \Delta E, \mathcal{F}, m(\pi^+\pi^-\pi^0) \equiv m_\omega, \mathcal{H} \}$,
(ii) $B^0 \rightarrow \eta' K^0_S$: $\{ m_{\text{ES}}, \Delta E, \mathcal{F} \}$,
(iii) $B^0 \rightarrow \eta' K^0_L$: $\{ \Delta E, \mathcal{F} \}$,
(iv) $B^0 \rightarrow \pi^0 K^0_S$: $\{ m_B, m_{\text{miss}}, L_2/L_0, \cos\theta_B \}$.

Here, $\mathcal{F}$ is a Fisher discriminant described below, and $\mathcal{H}$ is the cosine of the polar angle of the normal to the ω decay plane in the ω helicity frame, which is defined as the ω rest frame with polar axis opposite to the direction of the B. From Monte Carlo studies we find that including the η' mass, ρ mass, ρ helicity, or ω Dalitz plot coordinates does not improve the precision of the measurements of S and C.

In Fig. 1 we show PDFs for the signal and $q\bar{q}$ components for the ωK^0_S analysis, which are similar to those for the $\eta' K^0_S$ analysis. We parameterize the PDFs for the signal component using simulated events, while the background distributions are taken from sidebands of the data in the kinematic variables that exclude signal events. The parameters used in the PDFs are different for each mode.

For the background PDF shapes we use the following: the sum of two Gaussians for $\mathcal{Q}_{\text{sig}}(m_{\text{ES}})$ and $\mathcal{Q}_{\text{sig}}(\Delta E)$; a quadratic dependence for $\mathcal{Q}_{q\bar{q}}(\Delta E)$, $\mathcal{Q}_{\text{chrm}}(\Delta E)$, and $\mathcal{Q}_{q\bar{q}}(m_B)$; and the sum of two Gaussians for $\mathcal{Q}_{\text{chls}}(\Delta E)$. For $\mathcal{Q}_{q\bar{q}}(m_{\text{ES}})$ and $\mathcal{Q}_{q\bar{q}}(m_{\text{miss}})$ we use the function

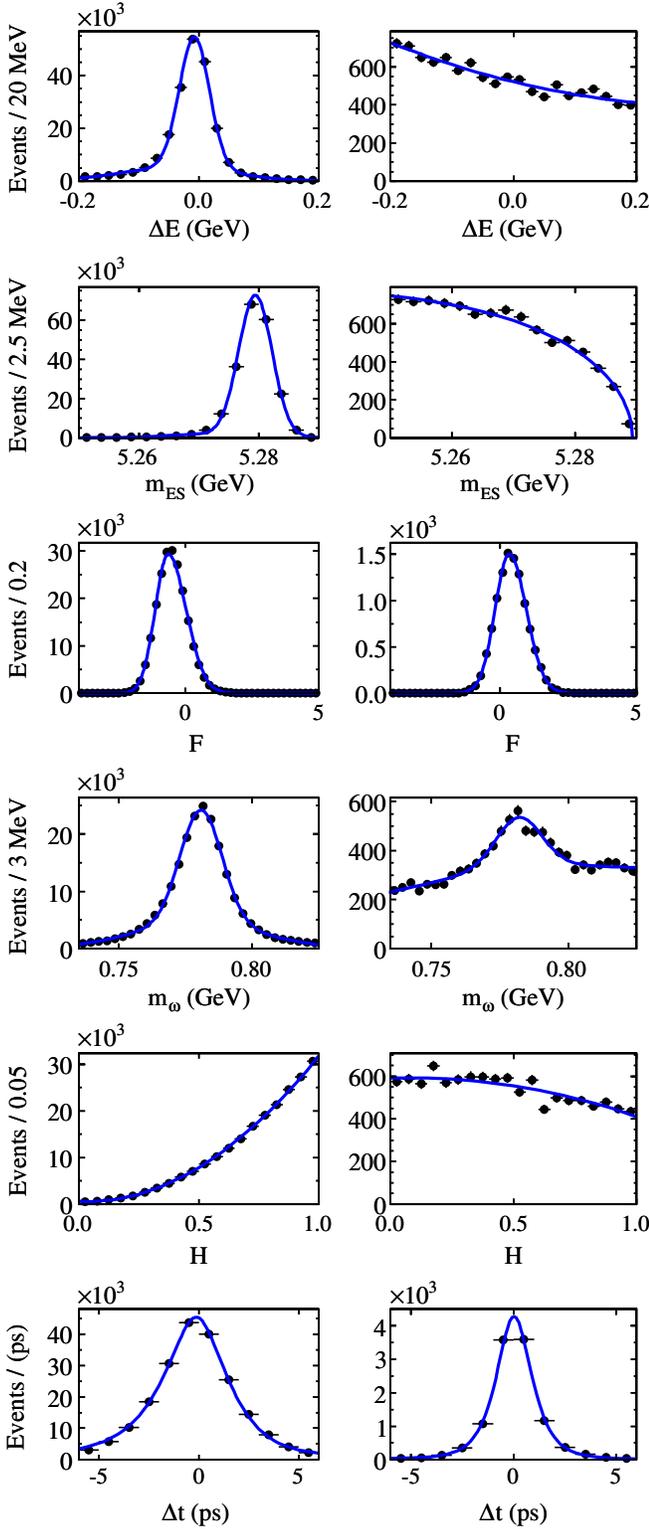$$f(x) = x\sqrt{1-x^2} \exp[-\xi(1-x^2)], \qquad (13)$$

FIG. 1 (color online). PDFs for ωK_S^0; from top to bottom ΔE, m_{ES}, $\mathcal{F}$, ω mass, $\mathcal{H}$, and Δt. In the left column we show distributions from signal Monte Carlo; in the right column we show distributions for the $q\bar{q}$ component, which are taken from sidebands of the data in the kinematic variables that exclude signal events.

with $x \equiv 2m_{ES}/\sqrt{s}$ ($2m_{miss}/\sqrt{s}$ for $\pi^0 K_S^0$) and ξ a free parameter [28], and the same function plus a Gaussian for $\mathcal{Q}_{chrm}(m_{ES})$ and $\mathcal{Q}_{chls}(m_{ES})$. For $\mathcal{Q}_{sig}(m_B)$ and $\mathcal{Q}_{sig}(m_{miss})$ we use the function

$$f(x) = \exp\left(\frac{-(x - \mu)^2}{2\sigma_{L,R}^2 + \alpha_{L,R}(x - \mu)^2}\right), \quad (14)$$

where μ is the peak position of the distribution, $\sigma_{L,R}$ are the left and right widths, and $\alpha_{L,R}$ are the left and right tail parameters. For $\mathcal{Q}_{q\bar{q}}(\Delta E)$ in the $\eta' K_L^0$ analysis, we use the function

$$f(x) = x(1 - x)^{-2} \exp[\xi' x], \quad (15)$$

where $x \equiv \Delta E - (\Delta E)_{min}$, with $(\Delta E)_{min}$ fixed to -0.01, and ξ' is a free parameter.

To reduce $q\bar{q}$ background beyond that obtained with the $\cos\theta_T$ requirement described above for ωK_S^0 and $\eta' K^0$ (and the θ_B and L_2/L_0 requirements for $\pi^0 K_S^0$), we use additional event topology information in the ML fit. The variables used include θ_B, L_0, L_2, and the angle with respect to the beam axis in the $Y(4S)$ frame of the signal B thrust axis (θ_S). For the $\pi^0 K_S^0$ analysis, we use $\cos\theta_B$ and the ratio L_2/L_0 directly in the fit, parameterized by a second-order polynomial and a seven-bin histogram, respectively. The parameters of the L_2/L_0 PDF depend on the tagging category c in the signal component. In Fig. 2 we show the PDFs for signal (background) superimposed on the
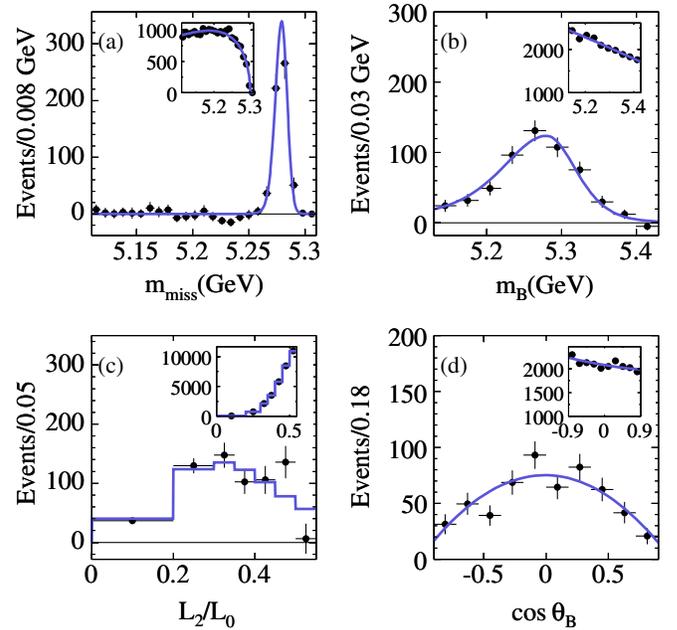

FIG. 2 (color online). Distribution of (a) m_{miss}, (b) m_B, (c) L_2/L_0, (d) $\cos\theta_B$, for signal (background-subtracted) events in data (points) from the $B^0 \to K_S^0 \pi^0$ sample. The solid curve represents the shape of the signal PDF, as obtained from the ML fit. The insets show the distribution of the data, and the PDF, for background (signal-subtracted) events.

distribution for data where background (signal) events are subtracted using an event weighting technique [29]. The bin widths of the L_2/L_0 histogram have been adjusted to be coarser where the background is small to reduce the number of free parameters of the PDF.

For the other decay modes we construct a Fisher discriminant $\mathcal{F}$, which is an optimized linear combination of L_0, L_2, $|\cos\theta_B|$, and $|\cos\theta_S|$. For the K_L^0 modes we also use the continuous output of the flavor tagging algorithm as a variable entering the Fisher discriminant. The coefficients used to combine these variables are chosen to maximize the separation (difference of means divided by quadrature sum of errors) between the signal and continuum background distributions of $\mathcal{F}$, and are determined from studies of signal MC and off-peak data. We have studied the optimization of $\mathcal{F}$ for a variety of signal modes, and find that a single set of coefficients is nearly optimal for all.

The PDF shape for $\mathcal{F}$ is an asymmetric Gaussian with different widths below and above the peak for signal, plus a broad Gaussian for $q\bar{q}$ background to account for a small tail in the signal $\mathcal{F}$ region. The background peak parameter is adjusted to be the same for all tagging categories c. Because $\mathcal{F}$ describes the overall shape of the event, the distribution for $B\bar{B}$ background is similar to the signal distribution.

For $\mathcal{Q}_{\mathrm{sig}}(m_\omega)$ we use the sum of two Gaussians; for $\mathcal{Q}_{q\bar{q}}(m_\omega)$ and $\mathcal{Q}_{\mathrm{chls}}(m_\omega)$ the sum of a Gaussian and a quadratic. For $\mathcal{Q}_{\mathrm{sig}}(\mathcal{H})$ and $\mathcal{Q}_{q\bar{q}}(\mathcal{H})$ we use a quadratic dependence, and for $\mathcal{Q}_{\mathrm{chls}}(\mathcal{H})$ a fourth-order polynomial. As described in Sec. IV, the resolution function in $\mathcal{T}_j(\Delta t)$ is a sum of three Gaussians for all fit components j. For $q\bar{q}$ background we use the same functional form $\mathcal{T}_j(\Delta t)$ as for signal, but fix the B lifetime τ to zero so that $\mathcal{T}_j(\Delta t)$ is effectively just the resolution model. For the signal and $B\bar{B}$ background components we determine the parameters of $\mathcal{Q}_{k,j}(x_k^i)$ from simulation, and the $q\bar{q}$ background parameters are free in the final fit. For the signal resolution function we fix all parameters to values obtained from the B_{flav} sample; we obtain parameter values from MC for the charm and charmless $B\bar{B}$ resolution models; we leave parameters of the Δt resolution model for $q\bar{q}$ free in the final fit.

For the ωK_S^0 and $\eta' K^0$ analyses, we use large control samples to determine any needed adjustments to the signal PDF shapes that have initially been determined from Monte Carlo. For m_{ES} and ΔE in ωK_S^0 and $\eta' K_S^0$, we use the decay $B^- \to \pi^- D^0$ with $D^0 \to K^- \pi^+ \pi^0$, which has similar topology to the modes under study here. We select this sample by making loose requirements on m_{ES} and ΔE, and requiring for the D^0 candidate mass $1845 < m_D < 1885$ MeV. We also place kinematic requirements on the D and B daughters to force the charmed decay to look as much like that of a charmless decay as possible. These selection criteria are applied both to the data and to MC. For $\mathcal{F}$, we use a sample of $B^+ \to \eta'_{\rho\gamma} K^+$ decays selected

with requirements very similar to those of our signal modes. From these control samples, we determine small adjustments (of the order of few MeV) to the mean value of the signal ΔE distribution. The means and widths of the other distributions do not need adjustment.

For the ω mass line shape, we use ω production in the data sidebands. The means and resolutions of the invariant mass distributions are compared between data and MC, and small adjustments are made to the PDF parameterizations. These studies also provide uncertainties in the agreement between data and MC that are used for evaluation of systematic errors. For the $\pi^0 K_S^0$ analysis, we apply no correction to the signal PDF shapes, but we evaluate the related systematic error as described in Sec. VIII.

C. Fit variables

For the ωK_S^0 analysis we perform a fit with 25 free parameters: S, C, signal yield, continuum background yield and fractions (6), and the background PDF parameters for Δt, m_{ES}, ΔE, $\mathcal{F}$, m_ω, and $\mathcal{H}$ (15). For the five $\eta' K_S^0$ channels we perform a single fit with 98 free parameters: S, C, signal yields (5), $\eta'_{\rho\gamma} K_S^0$ charm $B\bar{B}$ background yields (2), continuum background yields (5) and fractions (30), and the background PDF parameters for Δt, m_{ES}, ΔE, and $\mathcal{F}$ (54). Similarly, the two $\eta' K_L^0$ channels are fit jointly, with 34 parameters: S, C, signal yields (2), background yields (2), fractions (12), and PDF parameters (16). For the $\pi^0 K_S^0$ analysis we perform a fit with 36 free parameters: S, C, signal yield, the means of m_{miss} and m_B signal PDFs, background yield, background PDF parameters for Δt, m_B, m_{miss}, L_2/L_0, $\cos\theta_B$ (16), background tagging efficiencies (12), and the fraction of good events (2). For the signal, charm $B\bar{B}$, and charmless $B\bar{B}$ components the parameters τ and Δm_d are fixed to world-average values [24]; for the $B\bar{B}$ components S and C are fixed to zero and then varied to obtain the related systematic uncertainty as described below; for the $q\bar{q}$ model τ is fixed to zero.

D. Fit validation

We test the fitting procedure by applying it to ensembles of simulated experiments with $q\bar{q}$ and $B\bar{B}$ charmed events drawn from the PDF into which we have embedded the expected number of signal and $B\bar{B}$ charmless background events (with the expected values of S and C) randomly extracted from the fully simulated MC samples. We find biases (measured $-$ expected) for $S_{\omega K_S^0}$, $S_{\eta' K_S^0}$, $C_{\eta' K_S^0}$, $S_{\eta' K_L^0}$, and $C_{\eta' K_L^0}$ of 0.034 ± 0.010, 0.006 ± 0.006, -0.008 ± 0.005, -0.022 ± 0.014, and -0.013 ± 0.009, respectively. These small biases are due to neglected correlations among the observables, contamination of the signal by self-crossfeed, and the small signal event yield in ωK_S^0. We apply additive corrections to the final results for these biases. For $C_{\omega K_S^0}$, $S_{\pi^0 K_S^0}$, and $C_{\pi^0 K_S^0}$ we make no

TABLE III. Results of the fits. Signal yields quoted here include events with no flavor tag information. Subscripts for η' decay modes denote (1) $\eta'_{\eta(\gamma\gamma)\pi\pi}$, (2) $\eta'_{\rho\gamma}$, and (3) $\eta'_{\eta(3\pi)\pi\pi}$.

Mode	# events	Signal yield	$-\eta_f S_f$	C_f
ωK_S^0	17422	163 ± 18	$0.55^{+0.26}_{-0.29}$	$-0.52^{+0.22}_{-0.20}$
$\eta'_1 K^0_{\pi^+\pi^-}$	1470	472 ± 24	0.70 ± 0.17	-0.17 ± 0.11
$\eta'_2 K^0_{\pi^+\pi^-}$	22775	1005 ± 40	0.46 ± 0.12	-0.13 ± 0.09
$\eta'_3 K^0_{\pi^+\pi^-}$	513	171 ± 14	0.76 ± 0.26	0.05 ± 0.20
$\eta'_1 K^0_{\pi^0\pi^0}$	1056	105 ± 13	0.51 ± 0.34	-0.19 ± 0.30
$\eta'_2 K^0_{\pi^0\pi^0}$	27057	206 ± 28	0.26 ± 0.33	0.04 ± 0.26
$\eta' K_S^0$	52871	1959 ± 58	0.53 ± 0.08	-0.11 ± 0.06
$\eta'_1 K^0_L$	18036	386 ± 32	0.75 ± 0.22	0.02 ± 0.16
$\eta'_3 K^0_L$	6213	169 ± 21	0.87 ± 0.30	0.19 ± 0.25
$\eta' K^0_L$	24249	556 ± 38	$0.82^{+0.17}_{-0.19}$	$0.09^{+0.13}_{-0.14}$
$\pi^0 K_S^0$	21412	556 ± 32	0.55 ± 0.20	0.13 ± 0.13

correction but assign a systematic uncertainty as described in Sec. VIII.

VII. FIT RESULTS

Results from the fits for the signal yields and the *CP* parameters S_f and C_f are presented in Table III. In Figs. 3–9, we show projections onto the kinematic variables and Δt for subsets of the data for which the ratio of the likelihood to be signal and the sum of likelihoods to be signal and background (computed without the variable plotted) exceeds a mode-dependent threshold that optimizes the statistical significance of the plotted signal. In ωK_S^0 the fraction of signal events with respect to the total after this requirement has been applied is ~70%, while in $\eta' K_S^0$ and $\eta' K_L^0$, the fraction of signal events is in the (42–85)% and (22–55)% range, respectively, depending on the decay mode. In Fig. 3 we show the projections onto $m_{\rm ES}$ and ΔE for the ωK_S^0 analysis; in Fig. 4 we show the projections onto $m_{\rm ES}$ and ΔE for $\eta' K_S^0$; in Fig. 5 we show the ΔE projections for $\eta' K_L^0$. The corresponding information for $\pi^0 K_S^0$ is conveyed by the
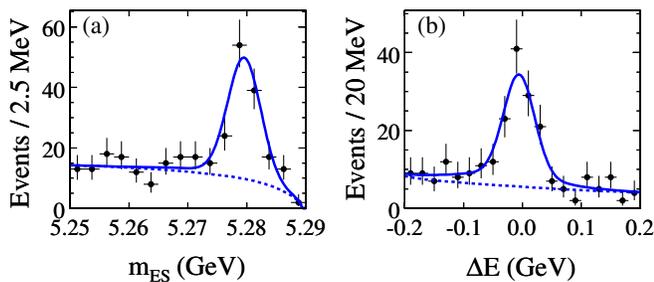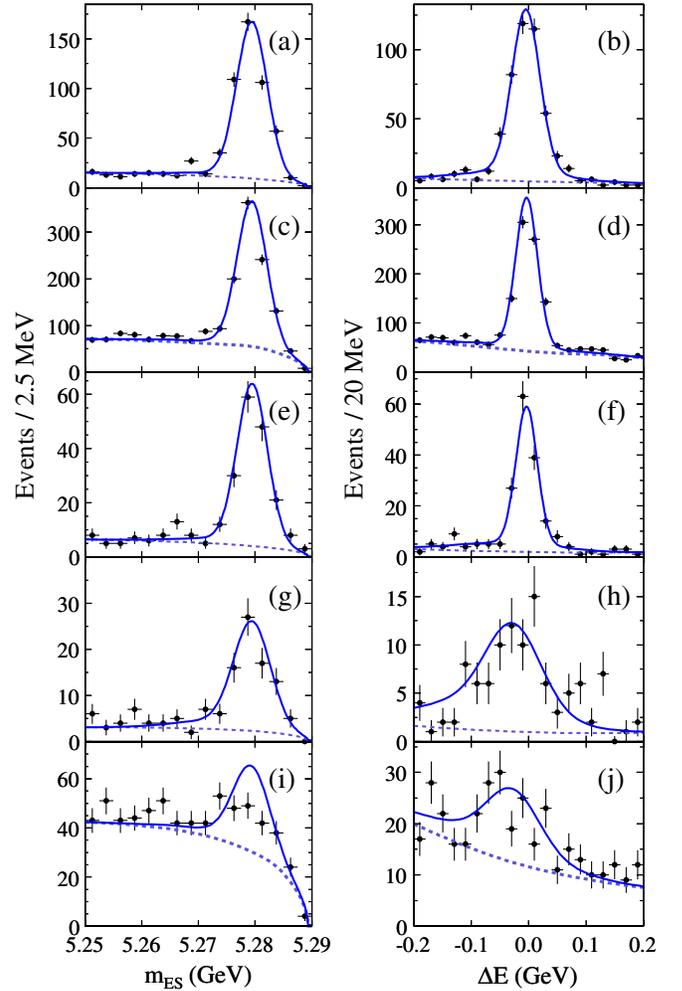

FIG. 4 (color online). Distributions for (a, b) $\eta'_{\eta(\gamma\gamma)\pi\pi} K^0_{\pi^+\pi^-}$, (c, d) $\eta'_{\rho\gamma} K^0_{\pi^+\pi^-}$, (e, f) $\eta'_{\eta(3\pi)\pi\pi} K^0_{\pi^+\pi^-}$, (g, h) $\eta'_{\eta(\gamma\gamma)\pi\pi} K^0_{\pi^0\pi^0}$, and (i, j) $\eta'_{\rho\gamma} K^0_{\pi^0\pi^0}$ projected (see text) onto $(m_{\rm ES}, \Delta E)$. The solid lines show the fit result and the dashed lines show the background contributions.

FIG. 3 (color online). Distributions for ωK_S^0 projected (see text) onto (a) $m_{\rm ES}$ and (b) ΔE. The solid lines show the fit result and the dashed lines show the background contributions.
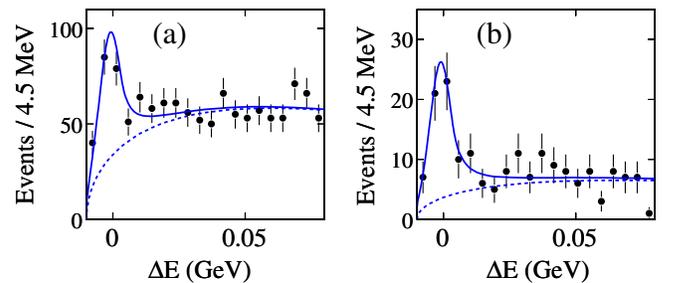

FIG. 5 (color online). Distributions for (a) $\eta'_{\eta(\gamma\gamma)\pi\pi} K^0_L$ and (b) $\eta'_{\eta(3\pi)\pi\pi} K^0_L$ projected (see text) onto ΔE. The solid lines show the fit result and the dashed lines show the background contributions.
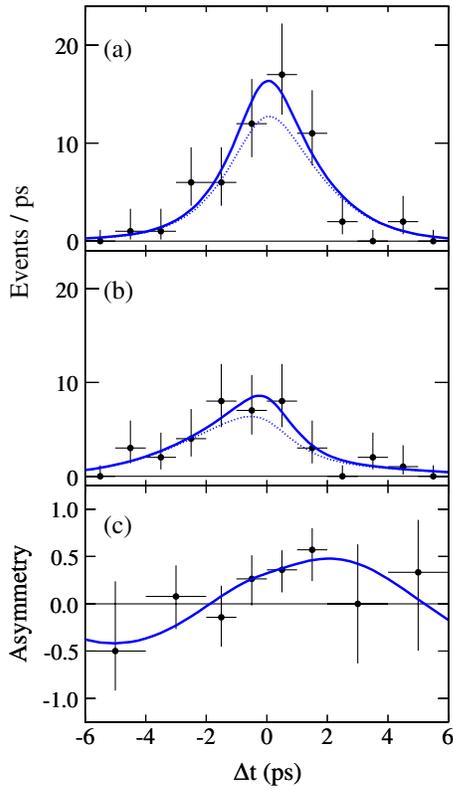
FIG. 6 (color online). Data and model projections for ωK_S^0 onto Δt for (a) B^0 and (b) $\bar{B}^0$ tags. We show data as points with error bars and the total fit function (total signal) with a the solid (dotted) line. In (c) we show the raw asymmetry, $(N_{B^0} - N_{\bar{B}^0})/(N_{B^0} + N_{\bar{B}^0})$ with a solid line representing the fit function.
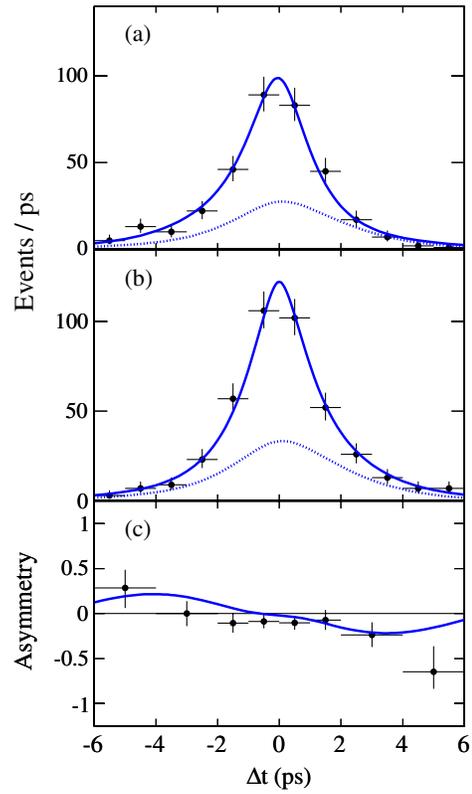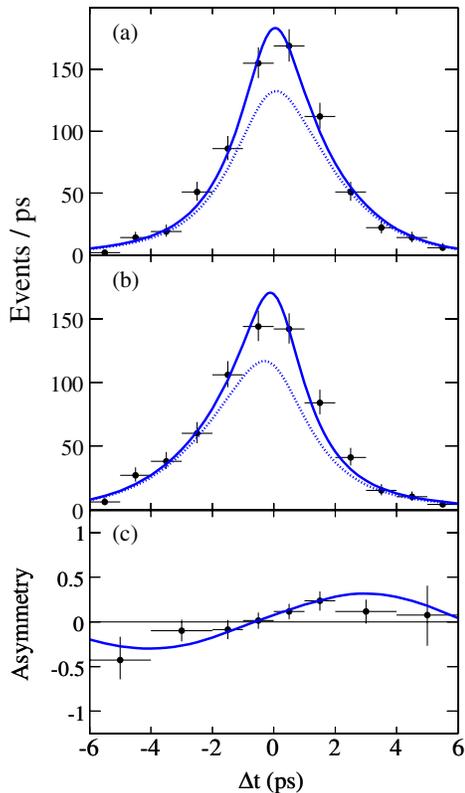

FIG. 8 (color online). Data and model projections for $B^0 \rightarrow \eta' K_L^0$ onto Δt for B^0 (a) and $\bar{B}^0$ (b) tags. Points with error bars represent the data; the solid (dotted) line displays the total fit function (total signal). In (c) we show the raw asymmetry, $(N_{B^0} - N_{\bar{B}^0})/(N_{B^0} + N_{\bar{B}^0})$; the solid line represents the fit function.
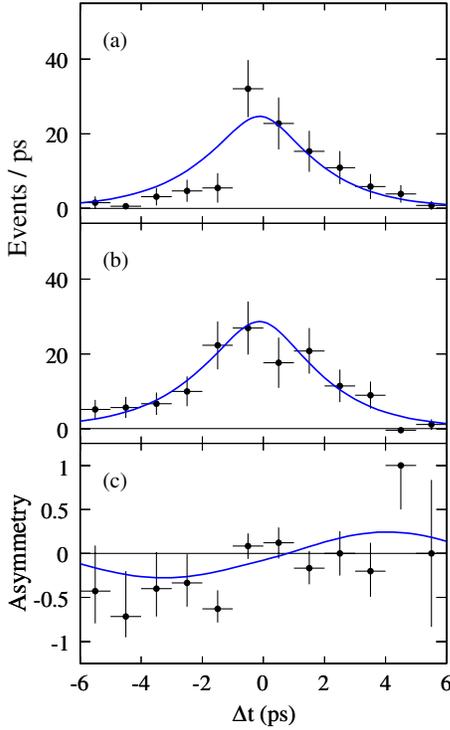

FIG. 7 (color online). Data and model projections for $\eta' K_S^0$ onto Δt for (a) B^0 and (b) $\bar{B}^0$ tags. Points with error bars represent the data; the solid (dotted) line displays the total fit function (total signal). In (c) we show the raw asymmetry, $(N_{B^0} - N_{\bar{B}^0})/(N_{B^0} + N_{\bar{B}^0})$; the solid line represents the fit function.

FIG. 9 (color online). Data and model projections for $\pi^0 K_S^0$ onto Δt for (a) B^0 and (b) $\bar{B}^0$ tags. Points with error bars represent the signal where background is subtracted using an event weighting technique [29]; the solid line displays the signal fit function. In (c) we show the raw asymmetry, $(N_{B^0} - N_{\bar{B}^0})/(N_{B^0} + N_{\bar{B}^0})$; the solid line represents the fit function.

background-subtracted distributions for m_B and m_{miss} in Fig. 2.

In Figs. 6–9, we show the Δt projections and the asymmetry $(N_{B^0} - N_{\bar{B}^0})/(N_{B^0} + N_{\bar{B}^0})$ for each final state. In the ωK_S^0, $\eta' K_S^0$, $\eta' K_L^0$, and $\pi^0 K_S^0$ analyses, we measure the correlation between S_f and C_f in the fit to be 2.9%, 3.0%, 1.0%, and -6.2%, respectively.

Crosschecks

We perform several additional crosschecks of our analysis technique including time-dependent fits for $B^\pm$ decays to the final states $\eta'_{\eta(\gamma\gamma)\pi\pi} K^\pm$, $\eta'_{\rho\gamma} K^\pm$, and $\eta'_{\eta(3\pi)\pi\pi} K^\pm$ in which measurements of S and C are consistent with zero. There are only small changes in the results when we do any of the following: fix $C = 0$ or $S = 0$, allow S and C to be different for each tagging category, remove each of the discriminating variables one by one, and allow the signal resolution model parameters to vary in the fit.

To validate the IP-constrained vertexing technique in $\pi^0 K_S^0$, we examine $B^0 \to J/\psi K_S^0$ decays in data where $J/\psi \to \mu^+ \mu^-$ or $J/\psi \to e^+ e^-$. In these events we determine Δt in two ways: by fully reconstructing the B^0 decay vertex using the trajectories of charged daughters of the J/ψ and the K_S^0 mesons (standard method), or by neglecting the J/ψ contribution to the decay vertex and

using the IP constraint and the K_S^0 trajectory only. This study shows that within statistical uncertainties of order 2% of the error on Δt, the IP-constrained Δt measurement is unbiased with respect to the standard technique and that the fit values of $S_{J/\psi K_S^0}$ and $C_{J/\psi K_S^0}$ are consistent between the two methods.

VIII. SYSTEMATIC UNCERTAINTIES

A number of sources of systematic uncertainties affecting the fit values of S_f and C_f have been considered.

We vary the parameters of the signal PDFs that are kept fixed in the fit within their uncertainty and take as systematic error the resulting changes of S_f and C_f. These parameters include τ and Δm_d, the mistag parameters w and Δw, the efficiencies of each tagging category, the parameters of the resolution model, and the shift and scale factors applied to the variables related to the B kinematics and event shape variables that serve to distinguish signal from background. The deviations of S_f and C_f for $\eta' K_S^0$ and $\eta' K_L^0$ for variations of τ and Δm_d are less than 0.002.

For the $\pi^0 K_S^0$ channel as an additional systematic error associated with the shape of the PDFs we also use the largest deviation observed when the parameters of the individual PDFs are free in the fit.

As a systematic uncertainty related to the fit bias on S_f and C_f we assign the statistical uncertainty on the bias obtained from simulated experiments during the fit validation. As explained in Sec. IV, we obtain parameters of the signal resolution model from a fit to the B_{flav} sample instead of from a fit to signal MC. We evaluate the systematic uncertainty of this approach with two sets of simulated experiments that differ only in the values of resolution model parameters (one set with parameters from the B_{flav} sample and one set with parameters from MC). We take the difference in the average S_f and C_f from these two sets of experiments as the related systematic error.

We evaluate the impact of potential biases arising from the interference of doubly Cabibbo-suppressed decays with the Cabibbo-favored decays on the tagside of the event [30] by taking into account realistic values of the ratio between the two amplitudes and the relative phases. For ωK_S^0 and $\eta' K^0$ we estimate using MC, published measurements, and theoretical predictions that conservative ranges of the net values for CP parameters in the $B\bar{B}$ background are $S = [0, 0.2]$ and $C = \pm 0.1$ for the charmless background and $S = \pm 0.1$ and $C = \pm 0.1$ for the charm background. We perform a fit in which we fix the parameters to these values and take the difference in signal CP parameters between this fit and the nominal fit as the systematic error.

For the ωK_S^0 and $\eta' K^0$ channels we also vary the amount of the charmless $B\bar{B}$ background by $\pm 20\%$. For $\pi^0 K_S^0$ we do not include a $B\bar{B}$ background component in the fit but we embed $B\bar{B}$ background events in the data sample and extract the peaking background from the observed change

TABLE IV. Summary of systematic uncertainties affecting S_f and C_f.

Source	$S_{\omega K_S^0}$	$C_{\omega K_S^0}$	$S_{\eta' K_S^0}$	$C_{\eta' K_S^0}$	$S_{\eta' K_L^0}$	$C_{\eta' K_L^0}$	$S_{\pi^0 K_S^0}$	$C_{\pi^0 K_S^0}$
Variation of PDF parameters	0.012	0.019	0.006	0.009	0.009	0.007	0.010	0.012
Bias correction	0.010	0.007	0.006	0.005	0.014	0.009	0.011	0.001
Interference from DCSD on tagside	0.001	0.015	0.001	0.015	0.001	0.015	0.001	0.015
$B\bar{B}$ background	0.009	0.010	0.009	0.005	-	-	0.005	0.001
Signal Δt parameters from B_{flav}	0.002	0.001	0.009	0.015	0.004	0.008	0.016	0.011
SVT alignment	0.011	0.003	0.002	0.003	0.004	0.004	0.009	0.009
Beam-spot position and size	0.000	0.000	0.002	0.001	0.004	0.003	0.004	0.002
Vertexing method	-	-	-	-	-	-	0.008	0.016
Self-crossfeed	-	-	0.004	0.001	0.001	0.004	-	-
Total	0.021	0.028	0.016	0.024	0.018	0.021	0.025	0.028

in the yield. We use this yield to estimate the change in S and C due to the *CP* asymmetry of the peaking background. We also measure the systematic error associated with the vertex reconstruction by varying within uncertainties the parameters of the alignment of the SVT and the position and size of the beam-spot.

We quantify the effects of self-crossfeed events in the $\eta' K^0$ analysis. For $\eta' K_S^0$ we perform sets of simulated experiments in which we embed only correctly reconstructed signal events and compare the results to the nominal simulated experiments (Sec. VI D) in which we embed both correctly and incorrectly reconstructed signal events. We take the difference as the systematic uncertainty related to self-crossfeed. For the $\eta'_{\eta(3\pi)\pi\pi} K_L^0$ analysis, in which we include a self-crossfeed component in the fit, we perform a fit in which we take parameter values for the self-crossfeed resolution model from self-crossfeed MC events instead of the nominal B_{flav} sample. We take the difference of the results from this fit and the nominal fit as the self-crossfeed systematic for $\eta' K_L^0$. The effects of self-crossfeed are negligible for ωK_S^0 and $\pi^0 K_S^0$.

Finally, for the $\pi^0 K_S^0$ analysis we examine large samples of simulated $B^0 \to K_S^0 \pi^0$ and $B^0 \to J/\psi K_S^0$ decays to quantify the differences between resolution function parameter values obtained from the B_{flav} sample and those of the signal channel; we use these differences to evaluate uncertainties due to the use of the resolution function extracted from the B_{flav} sample. We also use the differences between resolution function parameters extracted from data and MC in the $B^0 \to J/\psi K_S^0$ decays to quantify possible problems in the reconstruction of the K_S^0 vertex. We take the sum in quadrature of these errors as the systematic error related to the vertexing method.

The contributions of the above sources of systematic uncertainties to S_f and C_f are summarized in Table IV.

IX. S AND C PARAMETERS FOR $B^0 \to \eta' K^0$

As noted in Sec. I, the final states $\eta' K_S^0$ and $\eta' K_L^0$ have opposite *CP* eigenvalues, and in the SM, if $\Delta S_f = 0$, then

$-\eta_f S_f = \sin 2\beta$. We therefore compute the values of $S_{\eta' K^0}$ and $C_{\eta' K^0}$ from our separate measurements with $B^0 \to \eta' K_S^0$ and $B^0 \to \eta' K_L^0$, taking $-S_{\eta' K_L^0}$ in combination with $S_{\eta' K_S^0}$, and $C_{\eta' K_L^0}$ with $C_{\eta' K_S^0}$.

To represent the results of the individual fits, we project the likelihood by maximizing $\mathcal{L}$ (Sec. VI) at a succession of fixed values of S_f to obtain $\mathcal{L}(-\eta_f S_f)$. We then convolve this likelihood with a Gaussian function representing the independent systematic errors for each mode. The product of these convolved one-dimensional likelihood functions for the two modes, shifted in $-\eta_f S_f$ by their respective corrections (Sec. VI D), gives the joint likelihood for $S_{\eta' K^0}$. The likelihood for $C_{\eta' K^0}$ is computed similarly. Since the measured correlation between S_f and C_f is small in our fits (Sec. VII), we extract the central values and total uncertainties of these quantities from these one-dimensional likelihood functions. Applying the same procedure without the convolution over systematic errors yields the statistical component of the error. The systematic component is then extracted by subtraction in quadrature from the total error.

X. SUMMARY AND DISCUSSION

In conclusion, we have used samples of 121 ± 13 $B^0 \to \omega K_S^0$, 1457 ± 43 $B^0 \to \eta' K_S^0$, 416 ± 29 $B^0 \to \eta' K_L^0$, and 411 ± 24 $B^0 \to \pi^0 K_S^0$ flavor-tagged events to measure the time-dependent *CP* violation parameters

$$S_{\omega K_S^0} = 0.55^{+0.26}_{-0.29} \pm 0.02$$

$$C_{\omega K_S^0} = -0.52^{+0.22}_{-0.20} \pm 0.03$$

$$S_{\eta' K^0} = 0.57 \pm 0.08 \pm 0.02$$

$$C_{\eta' K^0} = -0.08 \pm 0.06 \pm 0.02$$

$$S_{\pi^0 K_S^0} = 0.55 \pm 0.20 \pm 0.03$$

$$C_{\pi^0 K_S^0} = 0.13 \pm 0.13 \pm 0.03,$$

where the first errors are statistical and the second systematic. These results are consistent with and supersede our

previous measurements [14–16]; they are also consistent with the world average of $\sin 2\beta$ measured in $B^0 \rightarrow J/\psi K_S^0$ [24].

[1] B. Aubert *et al.* (*BABAR* Collaboration), Phys. Rev. Lett. **89**, 201802 (2002); K. Abe *et al.* (Belle Collaboration), Phys. Rev. D **66**, 071102(R) (2002).

[2] N. Cabibbo, Phys. Rev. Lett. **10**, 531 (1963); M. Kobayashi and T. Maskawa, Prog. Theor. Phys. **49**, 652 (1973).

[3] Y. Grossman and M. P. Worah, Phys. Lett. B **395**, 241 (1997); D. Atwood and A. Soni, Phys. Lett. B **405**, 150 (1997); M. Ciuchini *et al.*, Phys. Rev. Lett. **79**, 978 (1997).

[4] M. Beneke and M. Neubert, Nucl. Phys. **B675**, 333 (2003).

[5] C.-W. Chiang, M. Gronau, and J. L. Rosner, Phys. Rev. D **68**, 074012 (2003); M. Gronau, J. L. Rosner, and J. Zupan, Phys. Lett. B **596**, 107 (2004).

[6] D. London and A. Soni, Phys. Lett. B **407**, 61 (1997).

[7] Y. Grossman, Z. Ligeti, Y. Nir, and H. Quinn, Phys. Rev. D **68**, 015004 (2003).

[8] M. Beneke, Phys. Lett. B **620**, 143 (2005).

[9] H. Y. Cheng, C-K. Chua, and A. Soni, Phys. Rev. D **72**, 014006 (2005); **71**, 014030 (2005); S. Fajfer, T. N. Pham, and A. Prapotnik-Brdnik, Phys. Rev. D **72**, 114001 (2005).

[10] A. R. Williamson and J. Zupan, Phys. Rev. D **74**, 014003 (2006).

[11] M. Gronau, J. L. Rosner, and J. Zupan, Phys. Rev. D **74**, 093003 (2006).

[12] H-Y. Cheng, C-K. Chua, and A. Soni, Phys. Rev. D **72**, 014006 (2005).

[13] A. J. Buras, R. Fleischer, S. Recksiegel, and F. Schwab, Phys. Rev. Lett. **92**, 101804 (2004); R. Fleischer, S. Jager, D. Pirjol, and J. Zupan, Phys. Rev. D **78**, 111501 (2008); M. Gronau and J. L. Rosner, Phys. Lett. B **666**, 467 (2008).

[14] B. Aubert *et al.* (*BABAR* Collaboration), Phys. Rev. D **74**, 011106 (2006).

[15] B. Aubert *et al.* (*BABAR* Collaboration), Phys. Rev. Lett. **98**, 031801 (2007).

[16] B. Aubert *et al.* (*BABAR* Collaboration), Phys. Rev. D **77**, 012003 (2008).

[17] K. F. Chen *et al.* (Belle Collaboration), Phys. Rev. Lett. **98**, 031802 (2007).

[18] K. F. Chen *et al.* (Belle Collaboration), Phys. Rev. D **76**, 091103 (2007).

[19] B. Aubert *et al.* (*BABAR* Collaboration), Nucl. Instrum. Methods Phys. Res., Sect. A **479**, 1 (2002).

[20] G. Benelli *et al.*, *Nuclear Science Symposium Conference Record* (IEEE, New York, 2005), Vol. 2, p. 1145.

[21] B. Aubert *et al.* (*BABAR* Collaboration), Phys. Rev. Lett. **93**, 131805 (2004).

[22] B. Aubert *et al.* (*BABAR* Collaboration), Phys. Rev. D **66**, 032003 (2002).

[23] S. Agostinelli *et al.*, Nucl. Instrum. Methods Phys. Res., Sect. A **506**, 250 (2003).

[24] Y.-M. Yao *et al.* (Particle Data Group), J. Phys. G **33**, 1 (2006).

[25] B. Aubert *et al.* (*BABAR* Collaboration), Phys. Rev. D **66**, 032003 (2002).

[26] B. Aubert *et al.* (*BABAR* Collaboration), Phys. Rev. D **71**, 111102 (2005).

[27] A. de Rújula, J. Ellis, E. G. Floratos, and M. K. Gaillard, Nucl. Phys. **B138**, 387 (1978).

[28] H. Albrecht *et al.* (ARGUS Collaboration), Phys. Lett. B **241**, 278 (1990).

[29] M. Pivk and F. R. Le Diberder, Nucl. Instrum. Methods Phys. Res., Sect. A **555**, 356 (2005).

[30] O. Long, M. Baak, R. N. Cahn, and D. Kirkby, Phys. Rev. D **68**, 034010 (2003).